ELSEVIER

Journal of Alloys and Compounds 469 (2009) 34–41

Journal of ALLOYS AND COMPOUNDS

www.elsevier.com/locate/jallcom

Hexagonal $TmMn_6Sn_4Ge_2$ investigated by neutron diffraction and ^{119}Sn Mössbauer spectroscopy

Laura K. Perry [a], D.H. Ryan [a], G. Venturini [b,*], B. Malaman [b]

[a] *Centre for the Physics of Materials and Physics Department, McGill University, 3600 University Street, Montréal, Quebec H3A 2T8, Canada*

[b] *Laboratoire de Chimie du Solide Minéral, Université Henri Poincaré-Nancy I, associé au CNRS (UMR 7555), B.P. 239, 54506 Vandoeuvre les Nancy Cedex, France*

Received 17 January 2008; accepted 4 February 2008
Available online 19 March 2008

Abstract

The hexagonal compound $TmMn_6Sn_4Ge_2$ has been investigated by neutron diffraction and ^{119}Sn Mössbauer spectroscopy. The location of Ge atoms on the 2(c) site has been confirmed. Above 230 K, an easy plane helimagnetic structure is stable and below 70 K an easy axis ferrimagnetic structure prevails. The magnetic moments at 2 K are $\mu_{Tm} = 6.93\ \mu_B$ and $\mu_{Mn} = 2.25\ \mu_B$. In the intermediate temperature range, we observed a tilting of the spiral plane. The intermediate magnetic structure is clearly observed by the ^{119}Sn local probe through a field distribution for the Sn(2e) site and a quadrupolar distribution for the Sn(2d) site. The change of the magnetocrystalline anisotropy of the Tm sublattice with respect to the easy plane observed in the parent stannide $TmMn_6Sn_6$ might be related either to a shortening of the Tm–Mn distances or to a deformation of coordination shell around the Tm atom, both being caused by the location of Ge atoms on the 2(c) site. The stabilisation of the ferrimagnetic structure at low temperature might be driven by stronger Tm–Mn interactions that result from the reduced Tm–Mn bond lengths.

Keywords: Rare-earth alloys and compounds; Transition metal alloys and compounds; Mössbauer spectroscopy; Neutron diffraction

1. Introduction

Recent studies of hexagonal $HfFe_6Ge_6$-type $REMn_6Sn_4Ge_2$ (RE = Sc, Y, Nd–Sm, Gd–Tm, Lu) have revealed interesting features [1]. In the case of the $TmMn_6Sn_4Ge_2$ compound, a spontaneous magnetisation is observed at low temperatures although the parent compounds $TmMn_6Ge_6$ and $TmMn_6Sn_6$ are characterized by a high temperature antiferromagnetic structure and a low temperature helimagnetic structure [2,3]. This suggests that, for this pseudo-ternary compound, a ferrimagnetic structure becomes stable at low temperature. Moreover, the measurement of a non-negligible coercive field at low temperature suggests that an easy axis anisotropy prevails in this temperature range. Since $TmMn_6Sn_6$ is characterized by an easy plane, this observation may indicate that the substitution of germanium for tin induces a change of the easy magnetisation direction. In order to better understand these phenomena we decided to investigate the properties of $TmMn_6Sn_4Ge_2$ using neutron diffraction. Recent investigations of $RMn_6Sn_{6-x}M_x$ compounds (M = Ga, In) by ^{119}Sn Mössbauer spectroscopy have shown that the transferred hyperfine fields onto the Sn nuclei were correlated to the direction of the Mn moments [4–6]. In the present compound $TmMn_6Sn_4Ge_2$ characterized by a temperature dependent moment reorientation, it was interesting to confirm these previous results.

2. Experimental methods

The compound was prepared starting from the stoichiometric amounts of thulium, manganese, tin and germanium pieces melted in an induction furnace. The resulting ingot was then annealed for 2 weeks at 1123 K. The quality of the sample was checked by powder X-ray diffraction analysis using an XPert Pro diffractometer (Cu Kα). The neutron diffraction patterns were recorded on the D1b apparatus ($\lambda = 2.52$ Å) at the Institut Laue-Langevin (ILL Grenoble) and the magnetic structures were refined with the FULLPROF software [7].

^{119}Sn Mössbauer spectra were collected in transmission mode on a constant acceleration spectrometer using a 0.4 GBq ^{119m}Sn $CaSnO_3$ source with the sample in a vibration-isolated closed-cycle refrigerator. A 25 μm Pd filter was used to absorb the Sn Kα X-rays also emitted by the source. The spectrom-

* Corresponding author. Tel.: +33 3 83 68 46 73; fax: +33 3 83 68 46 11.
E-mail address: Gerard.Venturini@lcsm.uhp-nancy.fr (G. Venturini).

0925-8388/$ – see front matter © 2008 Elsevier B.V. All rights reserved.
doi:10.1016/j.jallcom.2008.02.004

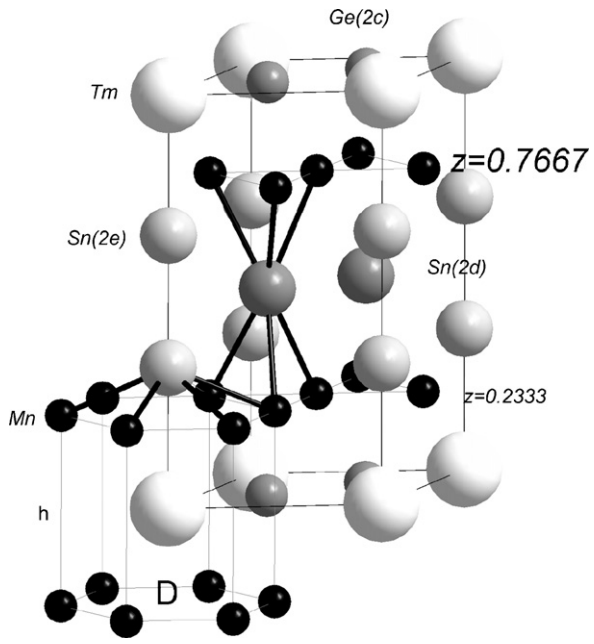

Fig. 1. Representation of the crystal structure of $TmMn_6Sn_4Ge_2$. The geometric features of the Mn_{12} hexagonal prism around the Tm atom are outlined and the directions of the Mn–Sn_{2e} and Mn–Sn_{2d} bonds are displayed.

eter was calibrated using a ^{57}Co Rh source and an α-Fe foil. Typical linewidths were 0.6 mm/s full width at half maximum (FWHM), consistent with a $CaSnO_3$ standard. Isomer shifts were measured relative to the same $CaSnO_3$ standard.

The spectra were fitted using a conventional non-linear least-squares minimization routine. As the magnetic hyperfine fields (B_{hf}) were much larger than the observed quadrupole splittings (Δ) at all temperatures used here, a simple first-order perturbation form was used to calculate line positions and intensities. The patterns were fitted with three magnetically split sextets corresponding to the three crystallographically distinct tin sites in the $HfFe_6Ge_6$-type structure, with an additional singlet near the centre of the spectra which we attribute to metallic tin.

3. Results

3.1. Neutron diffraction study of $TmMn_6Sn_4Ge_2$

3.1.1. Crystal structure

The neutron diffraction patterns of $TmMn_6Sn_4Ge_2$ sample are fully consistent with the $HfFe_6Ge_6$ type structure (Fig. 1). The refinement of the crystal structure has been done at 300 K, i.e. at a temperature where the magnetic peaks are rather weak and do not overlap with nuclear peaks (see below). Refinement of the occupation factors of the three tin sites clearly indicate an enhancement of the occupation factor corresponding to the 2(c) site. According to the relative values of the Fermi length of germanium (8.19 fm) and tin (6.22 fm), this means that the germanium atoms are mainly located on this site (Fig. 1). Refinement of the occupation factor of tin in 2(d) and 2(e) and germanium in 2(c) do not strongly deviate from the full occupation (Table 1).

The refined atomic coordinates show a strong decrease of the z_{Mn} value with respect to that measured in the pure ternary compound. This means that the Mn atom moves towards the 2(c) site occupied by the smaller Ge atom. At 300 K, the corresponding Mn–Ge distance (d_{MnGe} = 2.557 Å) is significantly smaller than the Mn–Sn ones (d_{MnSn} = 2.793 and 2.831 Å for the 2(d) and 2(e) sites, respectively) (Table 2). The shift of the Mn coordinate together with the decrease of the cell parameters also yield a significant shortening of the Tm–Mn distance (3.377 Å) with respect to that measured in the ternary stannide (3.545 Å) [8].

Table 1
Summary of the refined parameters of $TmMn_6Sn_4Ge_2$

	300 K	135 K	2 K
a (Å)	5.3934(4)	5.3768(6)	5.3692(4)
c (Å)	8.696(1)	8.673(1)	8.6684(9)
z_{Mn}	0.2333(8)	0.235(1)	0.236(1)
z_{Sn3}	0.3324(6)	0.332 (1)	0.333(1)
Occ_{Sn1}	1	1	1
Occ_{Ge2}	0.97(1)	0.97	0.97
Occ_{Sn3}	1	1	1
$\mu_{Mn(H1)}$ (μ_B)	1.28(3)	2.00(5)	–
$\mu_{Tm(H1)}$ (μ_B)	−0.51(9)	−2.92(14)	–
$\phi_{Mn(H1)}$	24.4(8)	12(1)	–
q_{z1}	0.2956(7)	0.2304(5)	–
$\mu_{Mn(H2)}$ (μ_B)	0.85(4)	–	–
$\mu_{Tm(H2)}$ (μ_B)	−0.26(14)	–	–
$\phi_{Mn(H2)}$	20(2)	–	–
q_{z2}	0.249(2)	–	–
θ_t (°)	0	90	–
$\mu_{Mn(H2)}$ (μ_B)	–	–	2.25(4)
$\mu_{Tm(H2)}$ (μ_B)	–	–	6.93(7)
θ_c (°)	–	–	0
μ_{Mn} (μ_B)	1.54(4)	2.01(4)	2.25(4)
μ_{Tm} (μ_B)	0.57(10)	2.92(12)	6.93(7)
R_{Bragg}; R_f; χ^2	1.68; 3.68, 5.96	1.36; 1.79, 14.7	2.02; 1.15, 24.6
R_{H1}; R_{H2}; R_F	13.6; 19.7; –	10.0; –; –	–; –; 3.77

3.1.2. Magnetic structures

Three long duration patterns have been recorded at 2, 135 and 300 K and short duration patterns have been recorded over the whole 2–300 K temperature range.

The diffraction patterns recorded at low temperature (T < 70 K) show only the characteristic nuclear lines of the $HfFe_6Ge_6$ structure. The weak intensity of the (0 0 1) line indicates that the moments are aligned along the c-axis in this

Table 2
Crystallographic properties of $TmMn_6Sn_4Ge_2$ and of the parent compounds $TmMn_6Sn_6$ and $TmMn_6Ge_6$

	$TmMn_6Sn_6$	$TmMn_6Sn_4Ge_2$	$TmMn_6Ge_6$
a (Å)	5.514	5.3934(4)	5.219
c (Å)	8.998	8.696(1)	8.139
c/a	1.6318	1.6123	1.5594
z_{Mn}	0.2476	0.2333(8)	0.2499
$z_{Sn(Ge)}$	0.3356	0.3324(6)	0.3458
$d_{Mn\text{-}2c}$(Å)	2.738	2.557	2.531
$d_{Mn\text{-}2d}$(Å)	2.773	2.793	2.532
$d_{Mn\text{-}2e}$(Å)	2.868	2.831	2.724
$d_{Tm\text{–}Mn}$(Å)	3.545	3.375	3.308
D (Å)	5.514	5.3934	5.219
h (Å)	4.455	4.057	4.068
h/D	0.808	0.752	0.779

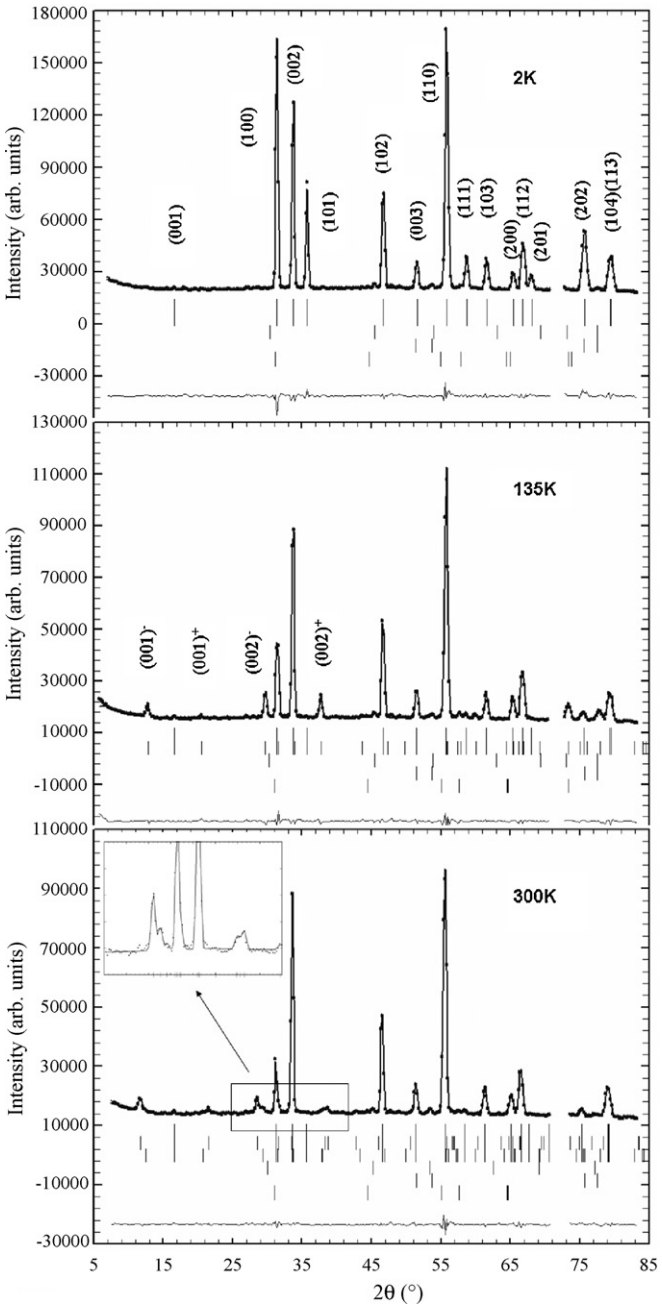

Fig. 2. Observed and calculated neutron diffraction spectra at 2, 134 and 300 K. Insert shows the splitting of the satellites at 300 K. The three lower lines of tiks correspond to the impurities: (from bottom to top) $MnSn_2$, Sn, Mn_2Sn.

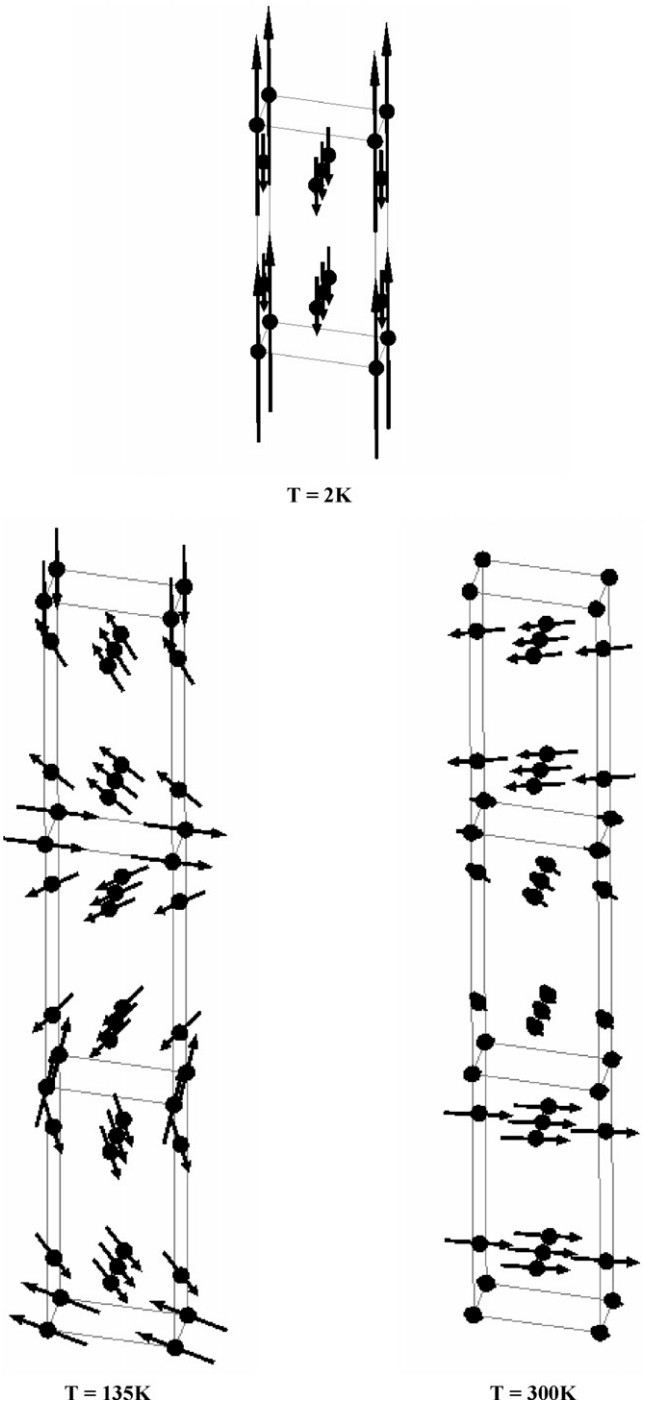

Fig. 3. Representation of the magnetic structures of $TmMn_6Sn_4Ge_2$ at 2, 135 and 300 K.

temperature range (Fig. 2). The refinements assuming a ferrimagnetic structure resulting from a collinear ferromagnetic manganese sublattice and an antiparallel arrangement of the thulium moment lead to low residual factors ($R = 3.7\%$). The magnetic structure is depicted in Fig. 3 and the refined parameters are gathered in Table 1. The thulium moment refined at 2 K is close to its free ion value.

Above 70 K, we observed a strong decrease of the ($h\,k\,l$) lines with $l = 1$ and simultaneously, the appearance of additional lines indexed as satellites of the nuclear ones with propagation vector $Q = (0, 0, q_z)$ (Fig. 4). Above 230 K, we observed an increase of the $(0\,0\,1)^{+-}$ satellites and the decrease of the $(1\,0\,0)^{+-}$ satellite (mixed with the nuclear (1 0 0) line). This is probably related to a change of the moment direction. Above $T \approx 250$ K, these satellites clearly split into at least two components, a feature which has been already observed in various other helimagnetic RMn_6Sn_6 compounds [2,9].

The refinements have been undertaken assuming a helimagnetic structure constituted of ferromagnetic (0 0 1) planes and a rotation of the moments in the successive (0 0 1) planes stacked

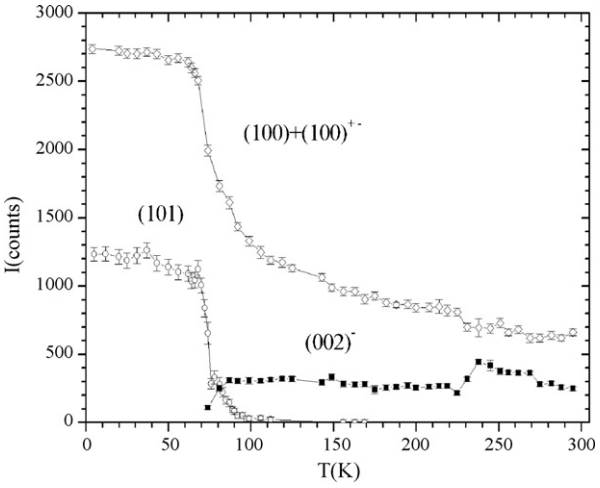

Fig. 4. Thermal variation of the intensities of several characteristic lines in $TmMn_6Sn_4Ge_2$ patterns.

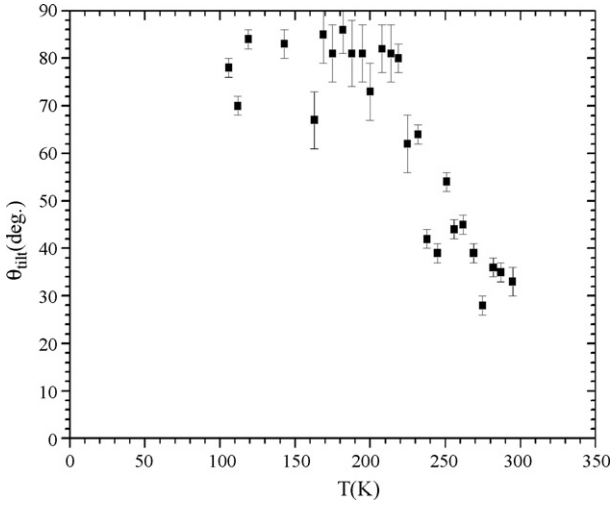

Fig. 6. Refined tilting angle of the helimagnetic structure of $TmMn_6Sn_4Ge_2$ as a function of the temperature.

along [0 0 1]. The phase angle of the thulium moments has been fixed to zero and the phase angles of the Mn moments lying in $z \approx 1/4$ and $z \approx 3/4$ to ϕ_{Mn} and $-\phi_{Mn}$, respectively. Owing to the variation of the relative intensities of the magnetic satellites, a possible tilting (θ_t) of the helical plane from the (0 0 1) plane has been also considered.

The refinements undertaken at 135 K lead to a tilt angle close to 90° but there is not a clear convergence of the free parameters although the residual factor drops to 12%. In the final refinement, the tilt angle was fixed to 90° yielding a residual factor $R = 10.2\%$. The results are gathered in Table 1 and a representation of the magnetic structure is given in Fig. 3. The final value of the phase angle leads to almost ferromagnetic Mn–Sn–Sn–Sn–Mn sheets. In the Mn–(Tm,Ge)–Mn slab, the Mn moment directions are not parallel and their average direction is opposite to that of the Tm moment consistent with the expected antiferromagnetic couplings between the two sublattices.

The refinements undertaken at 300 K assumed two helimagnetic phases, and for each of them we refined: q_z, the component of the propagation vector, the magnetic moments and the phase angles. The tilt angle has been constrained to be equal in both magnetic phases. The refinements lead to a tilt angle close to 24° but there is no clear convergence of the free parameters. The final refinements were undertaken by fixing the tilt angle to zero. In this case, convergence is reached and the reliability factors of the two magnetic phases are slightly improved thus indicating that, at room temperature, the helical plane lies in the (0 0 1) plane. The final parameters are gathered in Table 1 and the magnetic structure is depicted in Fig. 3.

The thermal variation of the magnetic moments, propagation vector, tilt angle θ_c and phase angle of the Mn moments has been checked using the short duration patterns. The results are gathered in Figs. 5–8. The Mn moment does not vary strongly in the whole temperature range except above 250 K, i.e. in the region close to the Néel point. On the contrary, the thulium moment is almost constant in the 2–50 K range, then it dis-

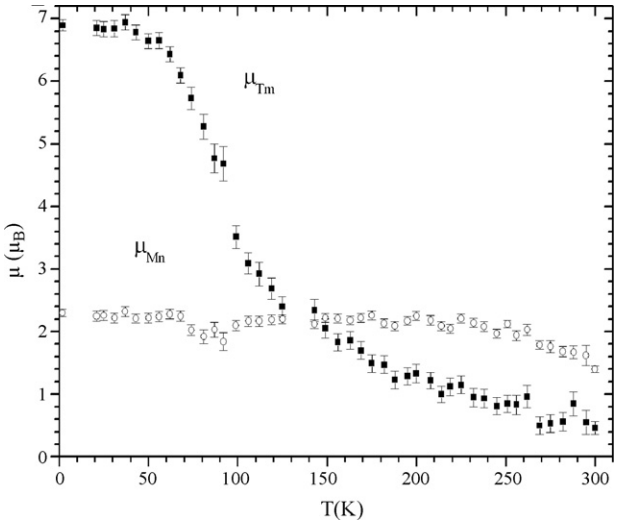

Fig. 5. Thermal variation of the Mn and Tm magnetic moment.

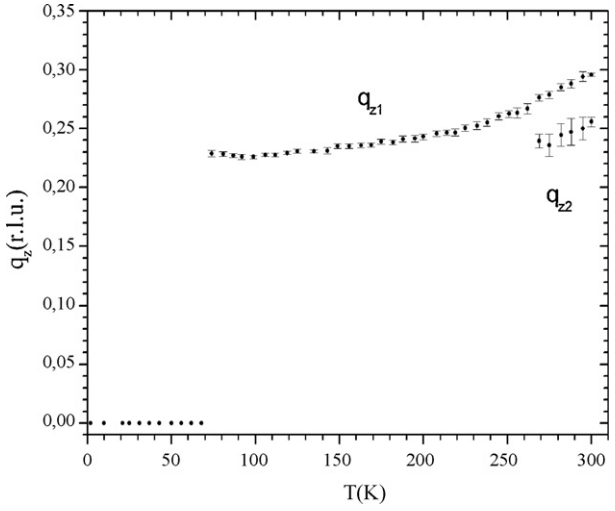

Fig. 7. Thermal variation of the q_z component of the propagating vectors.

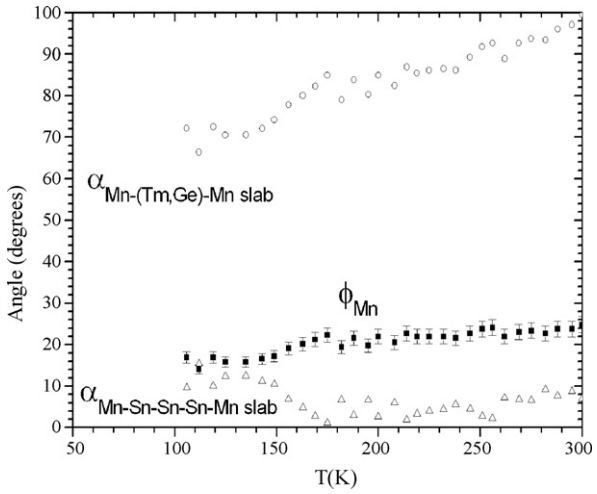

Fig. 8. Thermal variation of the refined phase angle ϕ_{Mn} and corresponding calculated angles between the Mn moments in the Mn–Sn–Sn–Sn–Mn and Mn–(Tm,Ge)–Mn slabs.

plays a strong reduction above 100 K and a weaker variation above this temperature. The tilt angle is almost constant and close to 90° from 100 to 220 K and shows a strong decrease above 230 K. This feature may be related to the variation of the intensity of any satellites as depicted in Fig. 4. The component q_z of the propagation vector slightly increases with the temperature and above 260 K we clearly observed a splitting

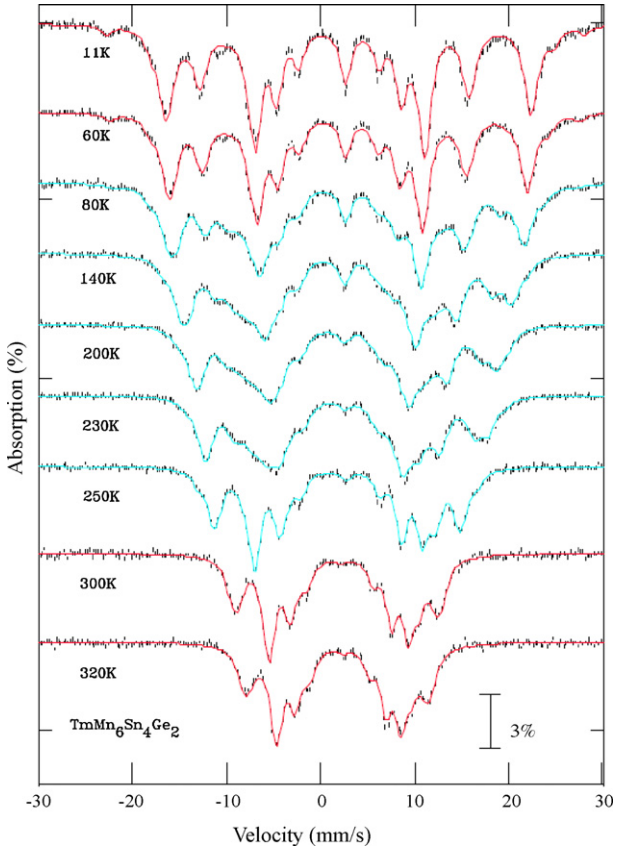

Fig. 9. Observed and calculated ^{119}Sn Mössbauer spectra as a function of the temperature.

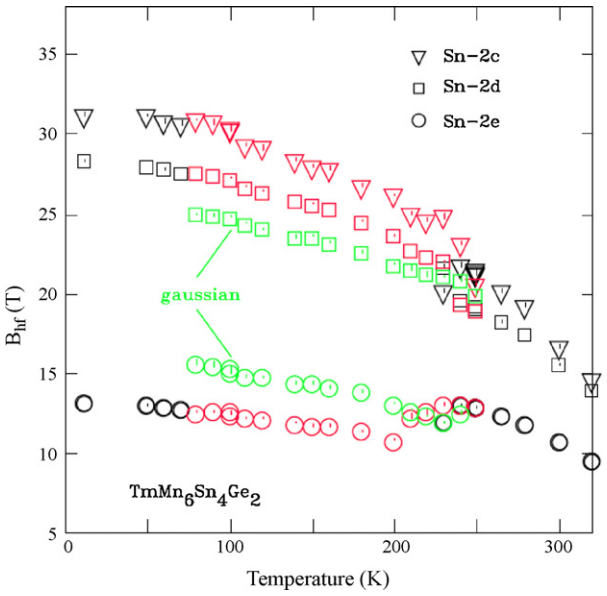

Fig. 10. Thermal variation of the hyperfine field of the ^{119}Sn sites.

into two components, the new one being close to 0.25 r.l.u. (Fig. 7). On another hand, the phase angle of the Mn moment decreases slowly and almost linearly from 300 to 160 K (Fig. 8). Both values enable us to calculate the angle between the Mn moments belonging to the successive planes along *c* (Fig. 8). It is observed that, in the temperature range 300–160 K, the angle within the Mn–Sn–Sn–Sn–Mn slab remains small and almost constant. This is consistent with a strong and positive Mn–Mn interlayer interaction. At the same time, we observed a decrease of the angle within the Mn–(Tm,Ge)–Mn slab, a feature which we attribute to increasing Tm–Mn antiferromagnetic interactions upon cooling. Below 160 K, the phase angle decreases more drastically yielding an opening of the angle within the Mn–Sn–Sn–Sn–Mn slab and a closing within the

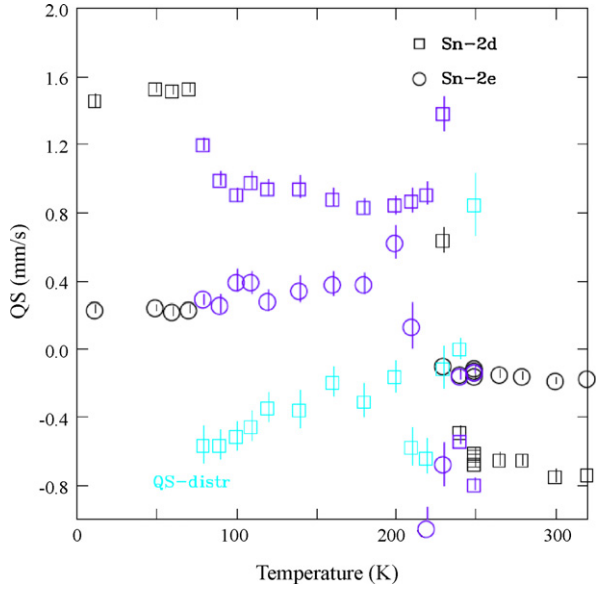

Fig. 11. Thermal variation of the quadrupolar splitting of the ^{119}Sn sites.

Mn–(Tm,Ge)–Mn slab. This frustrated situation is removed in the ferrimagnetic state that is stable at low temperature.

3.1.3. ^{119}Sn Mössbauer spectroscopy

The ^{119}Sn Mössbauer spectra at low ($T < 80$ K) and high ($T > 250$ K) temperatures were well fitted with three sextets and a singlet for the metallic tin impurity (Fig. 9). Site assignment is straightforward and proceeds by comparison with our earlier work on other $HfFe_6Ge_6$-type compounds [4–6]. The observed sequence of quadrupole shifts is: $|\Delta(\text{Sn-2d})| > |\Delta(\text{Sn-2c})| > |\Delta(\text{Sn-2e})|$, and with the moments oriented along the c-axis, below 80 K here, typical values are 1.6, 1.0 and 0.2 mm/s. The Sn-2d and Sn-2e components are found to have essentially equal areas, while the Sn-2c has approximately one-tenth the area of the other two components, consistent with the Sn site occupancies deduced from the neutron scattering data (Table 2).

The temperature dependence of the hyperfine fields (B_{hf}) presented in Fig. 10 shows that the field at the Sn-2e site *increases* on heating through the spin reorientation and that the changes at the other two sites are relatively small and largely obscured by the complexity of the reorientation process, however a modest *decrease* at the Sn-2d site is apparent. These changes are consistent with those expected from the anisotropic contribution to the hyperfine field for a c-axis to basal plane reorientation [5]. Similarly, comparison of the quadrupole shifts for the fully occupied Sn sites (2d and 2e) above and below the reorientation (Fig. 11) shows that Δ changes by a factor of -0.5 on heating, confirming that a full 90° rotation of the local field from the c-axis into the basal plane occurs in this system. Examination of $B_{hf}(T)$ (Fig. 10) and $\Delta(T)$ (Fig. 11) shows that the rotation starts at about 75 K and is complete by 250 K.

Unlike $ErMn_6Sn_{5.89}Ga_{0.11}$ [6] or $TbMn_6Sn_{6-x}Ga_x$ [4] where the reorientation proceeds by an abrupt 90° rotation, in $TmMn_6Sn_4Ge_2$ the process is far more complex, with an intermediate skewed helical phase. The abrupt reorientation is seen as a clean step in the hyperfine parameters and the spectral lines remain sharp [4–6], however the spectra of $TmMn_6Sn_4Ge_2$ for $80\text{ K} < T < 250$ K shown in Fig. 9 are severely broadened, indicating that the unique crystallographic environments of each of the three Sn sites do not remain magnetically unique in the skewed helical phase, and each experiences a range of magnetic effects.

We adopted the following model to fit the spectra in the skewed helical phase. The quadrupole shift at the Sn-2e site is quite small (Fig. 11), so the spin reorientation cannot have much effect on the spectra through changes in Δ, however the change in hyperfine field at this site in both this compound (Fig. 10), and others that we have studied [4–6] is relatively large, approaching 30%, we therefore used a Gaussian distribution of hyperfine fields to model the observed line broadening for the Sn-2e component. By contrast, the change in B_{hf} at the Sn-2d site is essentially zero, but the quadrupole shift changes from $\approx +1.5$ to ≈ -0.7 mm/s on heating through the spin reorientation, therefore, for the Sn-2d component we used a distribution of quadrupole shifts to fit the broadened lines. Finally, we found that broadened lines alone did not fully account for the observed spectral shape and we retained a sharp component for each site

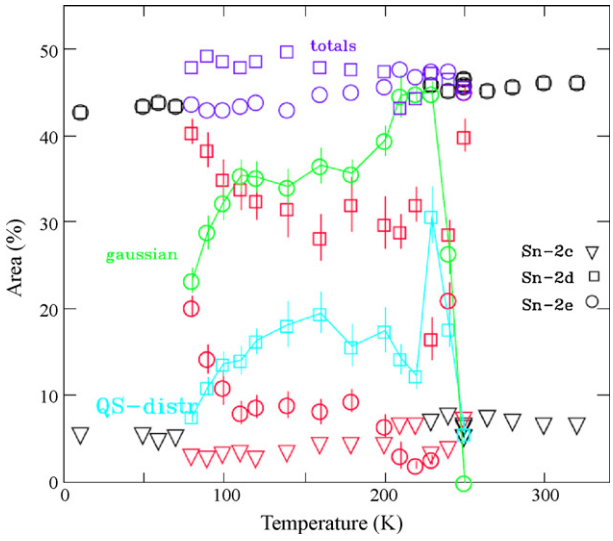

Fig. 12. Thermal variation of relative area of the ^{119}Sn sites.

with parameters that corresponded to the values observed at low temperatures and evolved towards those seen in the high temperature state. The sharp contributions accounted for about half (Sn-2d) to less than one quarter (Sn-2e) of the total site area and most likely reflect the limitations of the simple symmetric distributions used to model the spectral broadening at the two sites. In the high and low temperature phases where the magnetic order is collinear, we constrained the areas of the 2d and 2e components to be equal. This constraint was released for the complex forms used to fit the spectra in the skewed helical phase, however, the fits continued to return essentially equal areas at all temperatures (Fig. 12).

The decomposition of the fit used at 140 K is shown in Fig. 13. The weak central peak due to the metallic tin impurity is clear. In addition to the full fit, we also show the Sn-2d (large splitting) and Sn-2e (smaller splitting) components separately so that the distinct forms can be seen. Examining the average quadrupole shifts seen at the two components used to fit the contribution from the Sn-2d site (Fig. 11) we find that for much of the tem-

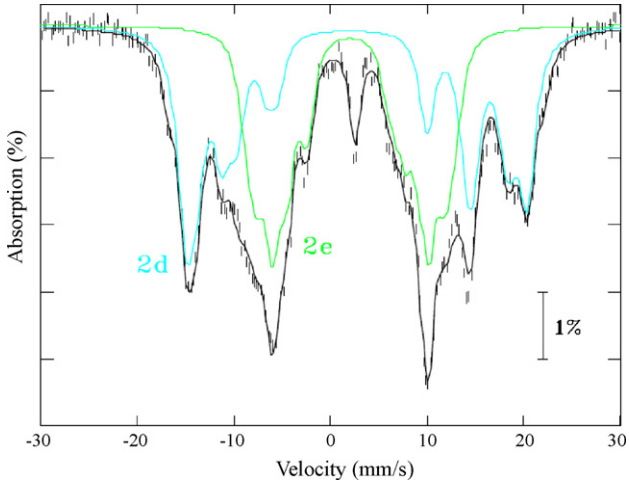

Fig. 13. ^{119}Sn Mössbauer spectrum at 140 K showing the decomposition of the fit.

perature range of the skewed helical phase, the two values are relatively stable at +0.90(5) mm/s (sharp) and −0.27(9) mm/s (broadened component). If we compare these values to that found when the moments are oriented parallel to the *c*-axis at low temperatures ($\Delta = 1.51(4)$ mm/s) and assume that the average quadrupole shifts reflect a well-defined average angle between the hyperfine magnetic field and the local electric field gradient (efg) through:

$$\Delta = \frac{eQV_{zz}}{4}(3\ \cos^2\theta - 1)$$

where θ is the angle between B_{hf} and the principal axis of the efg tensor (which is known to lie parallel to the *c*-axis in these compounds [4–6]), then we find that the sharp component yields an angle of 30(3)° between B_{hf} and the *c*-axis, while the broadened one yields and average angle of 62°.

4. Discussion

Our neutron diffraction and ^{119}Sn Mössbauer study of $TmMn_6Sn_4Ge_2$ provides interesting information. Firstly, we are able to show that it adopts an easy axis magnetic structure at low temperature, a feature which was assumed from the previous magnetisation measurements. This is consistent with the behaviour of the $TmMn_6Sn_{6-x}Ga_x$ compounds which also display an easy axis of the Tm moment [2]. In the case of the Ga substituted series, it has been suggested that the easy direction of the Tm moment might be related to the different valence of the gallium atoms and that their location in the equatorial plane of the dipyramid surrounding the Tm atoms might modify the charge distribution. This explanation cannot be used for the Ge substituted compounds and, more probably, the change of the easy direction in both the Ga and Ge substituted compounds might be related to the rearrangement of the atoms around the Tm site as a result of the smaller size of Ge or Ga atoms with respect to the Sn atom. This rearrangement yields two main modifications: firstly it leads to Tm–Mn distances that are significantly shorter than those measured in the pure ternary stannide, secondly it changes the shape of the hexagonal prism of manganese surrounding the Tm site. Table 2 gives the geometrical characteristic of the Mn coordination in the pure ternary $TmMn_6Sn_6$, $TmMn_6Ge_6$ compounds and in $TmMn_6Sn_4Ge_2$. The hexagonal prism is flatter in the substituted compound than in either of the ternary parent compounds. Whatever the origin of this easy axis anisotropy, it is likely that the tilt of the helical plane below 230 K is related to this anisotropy. Such skewed structures have been already observed in the ternary $TmMn_6Ge_6$ and $ErMn_6Ge_6$ germanides [3,10], a feature which suggests that the Er and Tm moments in germanides are also characterized by an easy axis anisotropy.

The stabilisation of the ferrimagnetic structure at low temperature, while the parent compound $TmMn_6Sn_6$ remains helimagnetic down to 2 K, is also a remarkable feature. The value of the propagation vector measured at 300 K is close to that of $TmMn_6Sn_6$ at the same temperature thus suggesting that the relative strengths of the competing interlayer Mn–Mn interactions are similar in both the compounds. Therefore the low temperature behaviour is probably driven by the increased Tm–Mn intreractions that result from the shorter Tm–Mn bonds in $TmMn_6Sn_4Ge_2$ compared with $TmMn_6Sn_6$. However, the effects of the easy axis anisotropy of the Tm moment cannot be ignored, as anisotropy may favour the collinear structure with respect to the helimagnetic structure.

Concerning the Mössbauer spectroscopy, the effects of the rotation of the moment are not as simple as previously observed in the other studied compounds. This is mainly due to the smoothed evolution of the magnetic structures with the transition from the easy plane helimagnetic structure to the easy axis ferrimagnetic structure via the skewed spiral structure. However, we observed that the hyperfine field on the Sn(2e) site decreases below 230 K when the spiral plane leaves the (0 0 1) plane. This is consistent with the previous observations made on the ferrimagnetic structures when the moment rotates from the (0 0 1) plane towards the [0 0 1] axis: since the direction of the Mn–Sn(2e) bonds is far away from the [0 0 1] direction, the anisotropic contribution to the transferred field is less efficient when the moments are aligned along the hexagonal axis.

^{119}Sn Mössbauer spectroscopy provides other information: although the refinements of the moment orientation from the neutron data do not enable a precise determination of this orientation, the change of the values of the quadrupolar splitting by a factor −2 confirms a 90° complete rotation of the moments.

Finally, the ^{119}Sn probe clearly experiences the tilting of the spiral plane through a distribution of fields and QS although this phenomenon is only related to weak changes of the intensities of the satellites lines in the neutron diffraction experiments.

5. Conclusion

The combination of neutron diffraction and ^{119}Sn Mössbauer spectroscopy enabled a detailed analysis of the magnetic properties of the pseudo-ternary compound $TmMn_6Sn_{\approx 4}Ge_{\approx 2}$. This compound is mainly characterized by a low temperature ferrimagnetic state which suggests enhanced Tm–Mn magnetic interactions and by an easy axis anisotropy of the thulium sublattice which should be related to the modification of the crystallographic environment of the thulium atom. To get a better understanding of these behaviours it will be now interesting to check the properties of other members of the series involving non-magnetic rare-earth elements or rare-earth elements characterized by different signs of the Steven's coefficient.

Acknowledgements

We are grateful to the Institut Laue Langevin (Grenoble) for the provision of research facilities. C.J. Voyer and E. Alonso-Ortiz (McGill) assisted with the collection of the ^{119}Sn spectra.

References

[1] G. Venturini, J. Alloys Compd. 398 (2005) 42–47.
[2] C. Lefèvre, G. Venturini, B. Malaman, J. Alloys Compd. 346 (2002) 84–94.
[3] P. Schobinger-Papamantellos, G. André, J. Rodriguez-Carvajal, J.H.V.J. Brabers, K.H.J. Buschow, J. Alloys Compd. 226 (1995) 113.

[4] L.K. Perry, D.H. Ryan, G. Venturini, J.M. Cadogan, J. Appl. Phys. 99 (2006), 08J302_1-3.
[5] L.K. Perry, D.H. Ryan, G. Venturini, Phys. Rev. B 75 (2007) 144417.
[6] L.K. Perry, D.H. Ryan, G. Venturini, J. Appl. Phys. 101 (2007), 09K504_1-4.
[7] J. Rodriguez-Carvajal, Physica B 192 (1993) 55.
[8] C. Lefèvre, G. Venturini, B. Malaman, J. Alloys Compd. 354 (1/2) (2003) 47–53.
[9] G. Venturini, D. Fruchart, B. Malaman, J. Alloys Compd. 236 (1996) 102.
[10] P. Schobinger-Papamantellos, G. André, J. Rodriguez-Carvajal, K.H.J. Buschow, J. Alloys Compd. 219 (1995) 176.